General Disclaimer

One or more of the Following Statements may affect this Document

- This document has been reproduced from the best copy furnished by the organizational source. It is being released in the interest of making available as much information as possible.

- This document may contain data, which exceeds the sheet parameters. It was furnished in this condition by the organizational source and is the best copy available.

- This document may contain tone-on-tone or color graphs, charts and/or pictures, which have been reproduced in black and white.

- This document is paginated as submitted by the original source.

- Portions of this document are not fully legible due to the historical nature of some of the material. However, it is the best reproduction available from the original submission.

Produced by the NASA Center for Aerospace Information (CASI)

04

(NASA-CR-158377) SINGLE FIBER STAR COUPLERS Final Report, 15 Aug. 1978 - 15 Feb. 1979 (Hughes Research Labs.) 54 p HC A04/MF A01 CSCL 20F

N79-20858

Unclas

G3/74 16686

Contract No. 955200

Final Report

March 1979

HUGHES

HUGHES AIRCRAFT COMPANY

SINGLE FIBER STAR COUPLERS

HUGHES RESEARCH LABORATORIES • MALIBU

SINGLE FIBER STAR COUPLERS

CONTRACT NUMBER 955200

for

Period 15 August 1978 through 15 February 1979

Program Manager

M.K. Barnoski

Principal Investigator

C.K. Asawa

Prepared for

JET PROPULSION LABORATORIES
4800 Oak Grove Drive
Pasadena, CA 91103

TABLE OF CONTENTS

Section	Page
SUMMARY	
INTRODUCTION	1
PLANAR STAR COUPLER DESIGN	3
PLANAR COUPLER PROCESSING	9
FIBER RIBBON ASSEMBLY	11
OPTICAL MEASUREMENTS	19
Refractive Index Profile	19
Optimization of the Fiber-to-Channel Coupling	19
Transmission Star Throughput	24
CONCLUSIONS	31
APPENDICES	
A. DESIGN OF PLANAR STAR COUPLERS FOR FIBER OPTIC SYSTEMS	33
B. PLANAR MULTIMODE COUPLERS FOR FIBER OPTICS	47

PAGE INTENTIONALLY BLANK

LIST OF ILLUSTRATIONS

Figure		Page
1	Eight-port transmission star coupler design	4
2	Calculated power throughput for (a) fiber-to-channel coupling and (b) fiber-to-channel-to-fiber coupling, using graded index parallel channel and graded index fiber	7
3a	End view of fiber ribbon connector	12
3b	Photograph of the input end of a star coupler with mating fiber ribbon connector	12
4	End view of ribbon of light fibers epoxied in etched silicon spacers	13
5a	Planar transmission star coupler with eight-fiber ribbon epoxied to each end	14
5b	Closeup of transmission star fiber ribbon connection	15
6	Planar transmission star in box with fiber connectors (cover removed)	16
7	Planar transmission star in box with fiber connectors	17
8	Interference microscope photograph of a star coupler cross section showing change of index of refraction	20
9	Power transmission ratios of constant width channel vs. channel widths for fiber-to-channel coupling and fiber-to-channel-to-fiber coupling	22
10	Channel-to-fiber coupling efficiency versus channel widths	23
11	Numbering of the channels of the transmission star coupler	27

SUMMARY

Hughes Research Laboratories has fabricated state-of-the-art planar star couplers for JPL for distributing optical radiation between optical fibers. These devices were fabricated by means of a new ion-exchange process. An 8x8 planar transmission star coupler has been packaged for evaluation purposes, with sixteen fiber connectors and sixteen pigtails. An additional transmission star coupler and an eight-port reflection star coupler have been fabricated and delivered; eight-fiber ribbons are rigidly attached to these couplers. A planar coupler with silicon guides and a parallel channel guide with pigtails have been fabricated and delivered. Optical measurements of the transmission star couplers have been made and are included in this final report.

INTRODUCTION

Low optical attenuation has made the optical fiber waveguide the leading contender as a transmission medium for many future communication and data handling systems. Low loss fibers have significant advantages over metallic conductors, including large bandwidth, small size and weight, immunity from crosstalk, ground loops and electromagnetic interference. Optical fibers thus appear to be an ideal medium for communication and data links operating in harsh environments such as experienced by spacecraft.

Development of specific components are required to take full advantage of optical fiber links. Such a component is the optical data distribution device, or coupler, which partitions radiation contained in one fiber to other fibers. This contract was directed towards fabricating state-of-the-art couplers for performing the data distribution task. We have fabricated a number of such couplers and have delivered the best planar couplers that we have fabricated to date on this contract. The design of the coupler, the chemical process used, the assembly process, and the optical measurement made on the delivered items are described here.

PRECEDING PAGE BLANK NOT FILMED

PLANAR STAR COUPLER DESIGN

The design of the transmission star coupler delivered under this contract is shown in Figure 1. The planar star is shown together with the interconnecting ribbons of eight fibers. The planar star consists of the intermediate channel waveguides, expansion and collecting horns, and the mixing region. These areas are processed by ion exchange and have a higher refractive index than the adjoining substrate, thereby permitting light guidance in these regions.

The geometric design for equal distribution of light from one fiber into the fibers at the other end of the star was determined by a computer ray tracing program. The computer program is described in detail in Appendix A. A step refractive index profile was assumed for the waveguide structure. As many as 10,000 rays were launched and tracked through the planar structure during the computer program. The computer program determined the number of rays partitioned into each exit port as the parameters (horn angle, intermediate channel width and spacing, mixing length) of the planar structure were varied. The program also summed the number of rays lost from the waveguide.

The calculations and practical considerations of fiber size resulted in a planar transmission star with the following dimensions:

Length of star, 10 cm,

Width of star, 0.2 cm,

Intermediate channel width (mask opening), 47 μm,

Separation of channel, center-to-center, 242 μm,

Angle of horn, 2°,

Length of mixing region, 8 cm.

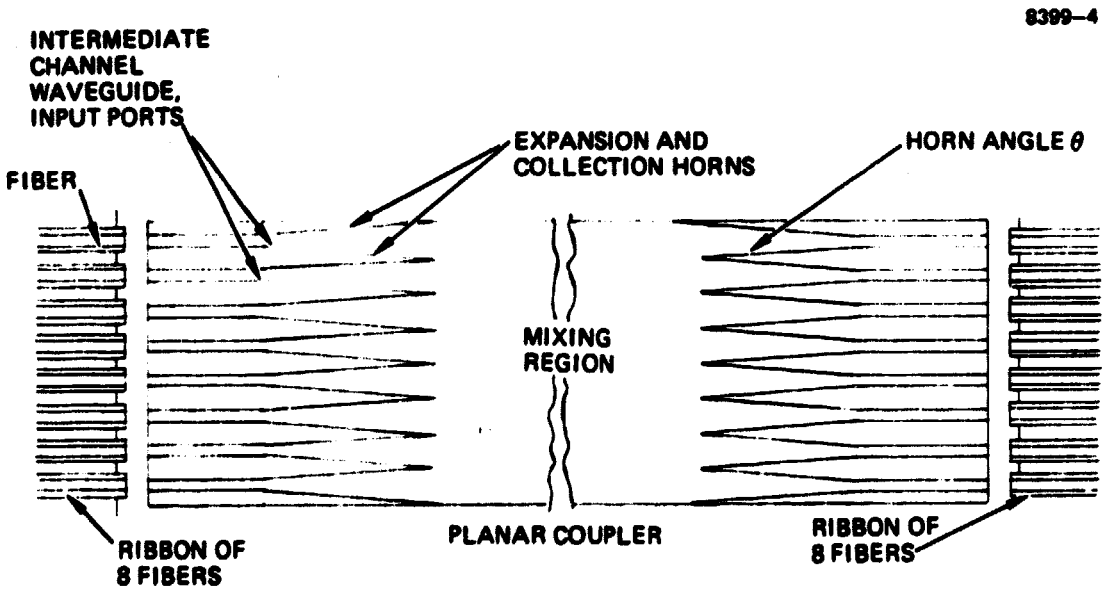

Fig. 1. Eight-port transmission star coupler design.

The star structure was ion-exchanged into a plate glass substrate. Although the step refractive index assumption is not realized in the ion exchange process, the ray tracing computer calculation (with step index profile) served as a guide in the design of the star. With the dimensions given above, the computer result with step index profile predicts a nearly equal partitioning of rays into the exit ports with a loss of ∿20%. The observed partitioning in a fabricated device, however, deviates from this. It then became clear that computer programs must consider the actual index profile. To this end, we initiated a ray tracing calculation (under Hughes IR&D) for a parallel channel with a graded index profile, where the input and output fibers also have index profile. The results are encouraging. The calculated throughput of the channel appears to correlate closely with the measured throughput.

A brief description of the ray tracing program for the parallel channel graded index structure is described here. We have computed the throughput power due to coupling a graded index fiber to graded parallel channel to graded index fiber. This theoretical result serves as a guideline for evaluating planar couplers fabricated by the single ion exchange process.

The assumptions and procedures used in the computer program are:

The ion exchanged waveguide has been modeled as a stepwise graded index structure consisting of 20 approximately elliptically shaped layers, each layer differing in refractive index. The refractive index varies linearly with layer depth from 1.532 at the ion exchange interface to 1.523 at the deepest layer. The length of the minor axis of an elliptical layer is taken to be twice the channel depth of that layer. The length of the major axis of each of the elliptical layer is set equal to the opening of the photomask (40 μm) plus the length of the mirror axis. The largest ellipse has a minor axis equal to twice the maximum waveguide depth.

The graded index fiber to which we couple the planar structure is assumed to have the following properties, as a source of rays to the planar structure:

1) Ray density over the core surface is uniform,

2) The maximum angular spread of the rays varies from the maximum guide numerical aperture at the center of the core NA(0) to zero spread at the core edge, in accordance with the formula

$$NA(r) = (1 - \alpha r^2)\ NA(0)$$

where r is the radial distance from the center of the core. The fiber NA(0) is assumed to be 0.2.

The results of the calculations are shown in Figure 2 where the coupled output power is graphed as a function of the relative position of the fiber to the planar channel. The upper two curves describe the fractional power at the exit (right) end of the channel due to radiation coupled from the fiber. The dotted line represents the output for a channel depth of three core radii, and the continuous line the output for a depth of two core radii. The maxima occurs when the ratio of the core center to surface distance ÷ core radius is unity, i.e., when the upper surface of the fiber core is at the same level as the channel surface.

The lower two curves of Figure 2 show the power coupled from the graded index fiber to the channel and then to the output fiber to the right. The upper continuous curve shows the output when the planar channel is two core radii deep, the dotted curve the output for a channel three core radii deep. The results suggest that the channel depth should be less than or equal to the core diameter for maximum power throughput. The maxima of the upper curve occurs when the upper surface of the core is slightly above the planar surface; approximately 55% of the input light should then be captured in the modes of the exit fiber.

It is clear that ray tracing through a structure such as the transmission star requires a somewhat more complex program than that for the parallel channel.

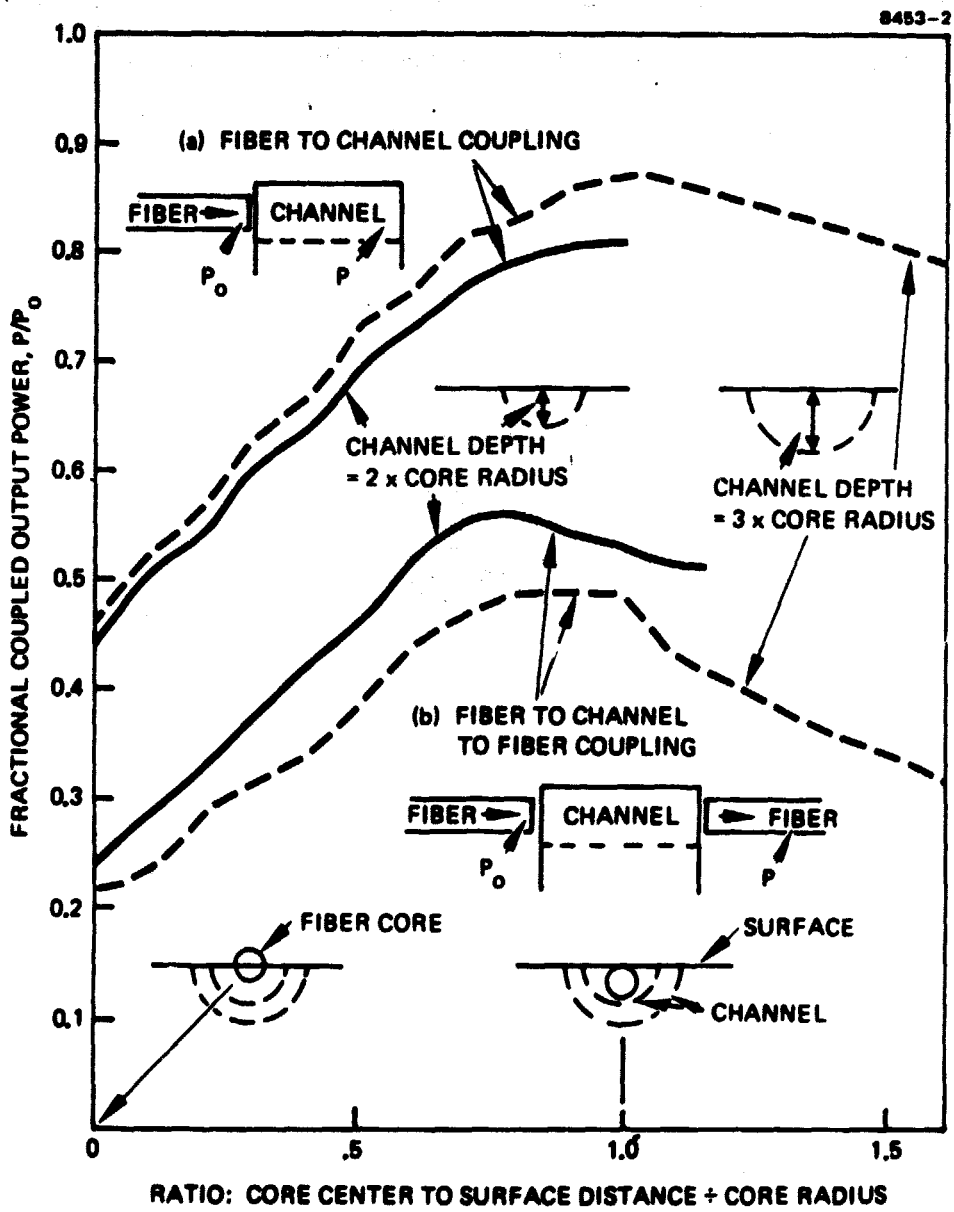

Fig. 2. Calculated power throughput for (a) fiber-to-channel coupling and (b) fiber-to-channel-to-fiber coupling, using graded index parallel channel and graded index fiber. Fiber radius = 31.25 μm; channel Δn = 0.009; graded index fiber NA = 0.2; 40 μm mask opening.

Nevertheless, we expect to address this problem in the immediate future in order to be able to correlate with the experimental results and to design improved stars and other planar devices.

PLANAR COUPLER PROCESSING

The ion-exchange process for fabricating the planar devices are described here. Eight-port transmission star couplers were fabricated by the process described in Appendix B. Aluminum films were evaporated on microscope or plate glass slides, then photoetched with open area corresponding to the planar star design described above. The slide was then dipped in a molten solution of Li_2SO_4-K_2SO_4 at 585°C for twenty (20) minutes to ion-exchange Na of the glass with Li of the melt. The slides were then sawed, ground and polished.

We have fabricated over fifty experimental star couplers using this procedure. Most of these were fabricated to test the ion-exchange exposure (temperature and time) and to test the photolithographic process. The earlier stars exhibited considerable scattering and loss. We examined the star coupler fabrication process in further detail to determine the sources of loss. The result has been an improvement in the quality of the star couplers. First, we determined that, for earlier fabrications, the temperature controller for the Li_2SO_4-K_2SO_4 melt was not properly calibrated, yielding a 20°C higher temperature than indicated. The higher temperature tends to corrode the Al masks more readily resulting in poorly formed guides. The temperature controller was recalibrated. Secondly, we have changed from negative to positive photoresists, using a dark field mask. The photoresist is now dipcoated, resulting in more uniform layer of photoresist on the aluminum and therefore more uniform etching. (Previously, spin coating of resist on the long samples resulted in a wavy, non-uniform photoresist layer.) The result has been a clean aluminum mask formation on the glass. More importantly, the use of positive photoresist process has eliminated the polymerized photoresist which remains on the aluminum surface with the negative resist process. It is

possible that during previous processing the polymerized photoresist had decomposed into products obscuring the star channels and resulting in incomplete ion exchange.

We fabricated two sets of ten 8x8 transmission star couplers, one set with negative resist and one set with positive resist. Various temperatures and ion exchange immersion times were used. The results were dramatically different. The negative resist couplers exhibited poor light transmission. The positive resist process has resulted in the best star coupler fabricated to date with throughput varying from better than -9 dB to -11 dB.

FIBER RIBBON ASSEMBLY

Two ribbons of eighteen (18) fibers (including fibers as spacers) to mate with the 8-channel star were fabricated. The cross section of one of the ribbons is shown in Figure 3a. Assuming that the fiber diameters were constant at 125 μm, an eight-port star mask was specified with interchannel spacing of 250 μm. Figure 3b illustrates dimensional mismatch arising from variations in fiber diameter and improper mask dimensions; the fiber spacings are greater than the channel spacings. Due to fluctuations in fiber diameter, the above ribbon fabrication procedure has been discontinued and replaced with a new process. We now use etched silicon alignment grooves to fabricate the fiber ribbon.

We successfully fabricated several ribbons of eight fibers for mating with the 8x8 planar star couplers. Etched silicon channels or spacers were fabricated by a process used in semiconductor technology. Etching of Si in the 100 direction proceeds at a fast rate relative to other directions. Channel masks with openings to match the dimensions of the star mask channels were fabricated. Using these masks, deep V grooves were etched into Si for aligning the fibers. Eight fibers were then inserted into the etched silicon channels and epoxied into place; the end of the unit was then ground and polished. Figure 4 shows the end view of the ribbon of eight fibers.

The ribbons of eight fibers were then carefully positioned at the ends of the eight-port transmission star coupler for maximum light throughput. The ribbons were then epoxied into place to form a rigid unit, as shown in Fig. 5a,b. One such unit was then boxed with connectors at the Hughes Connector Division in Irvine, Figures 6 and 7. (This unit is a prototype [or brassboard] and does not suggest any final packaging design.)

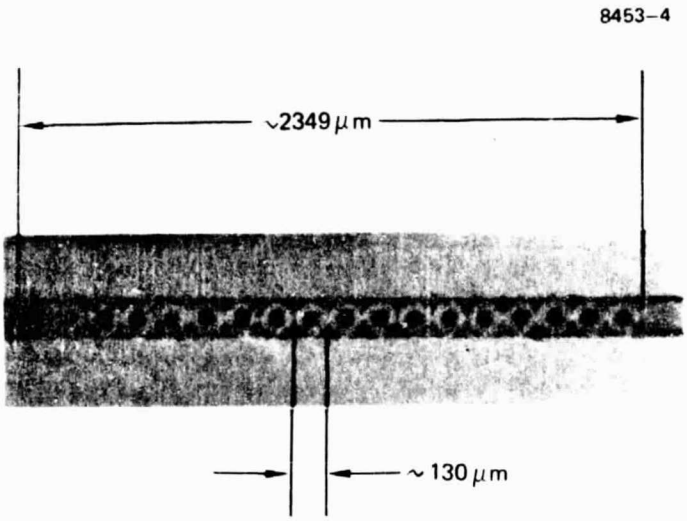

Fig. 3a. End view of fiber ribbon connector.

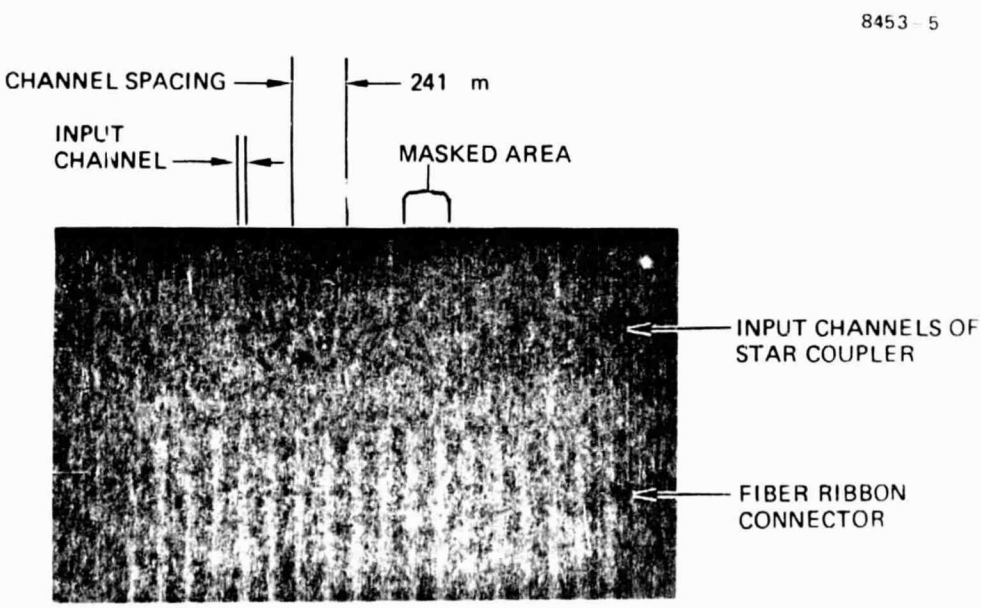

Fig. 3b. Photograph of the input end of a star coupler with mating fiber ribbon connector. Note alignment mismatch.

ORIGINAL PAGE IS
OF POOR QUALITY

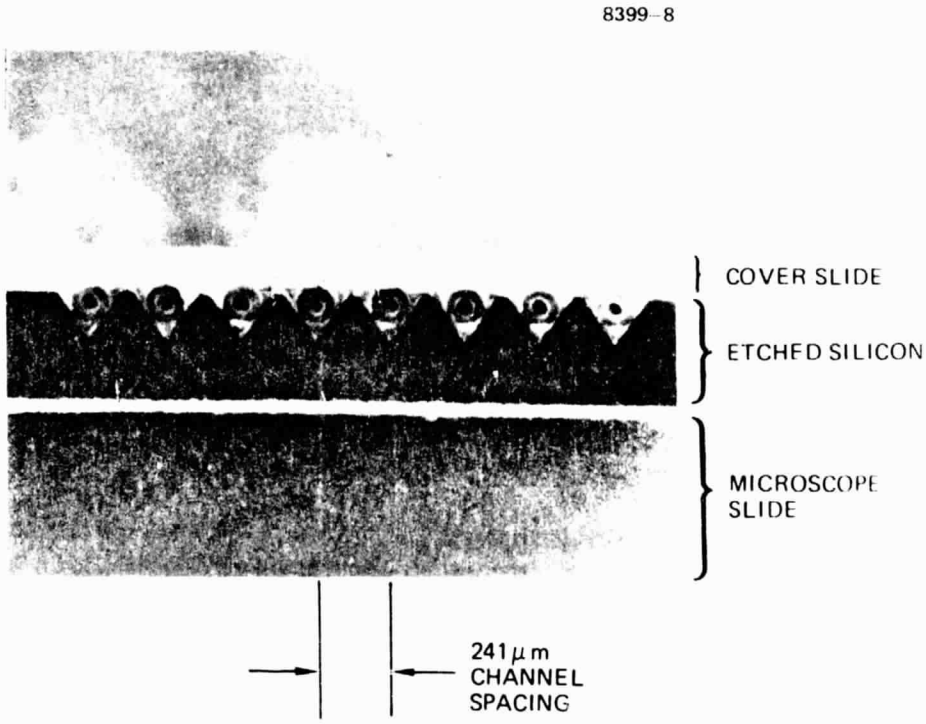

Fig. 4. End view of ribbon of light fibers epoxied in etched silicon spacers.

M12841

8453-6

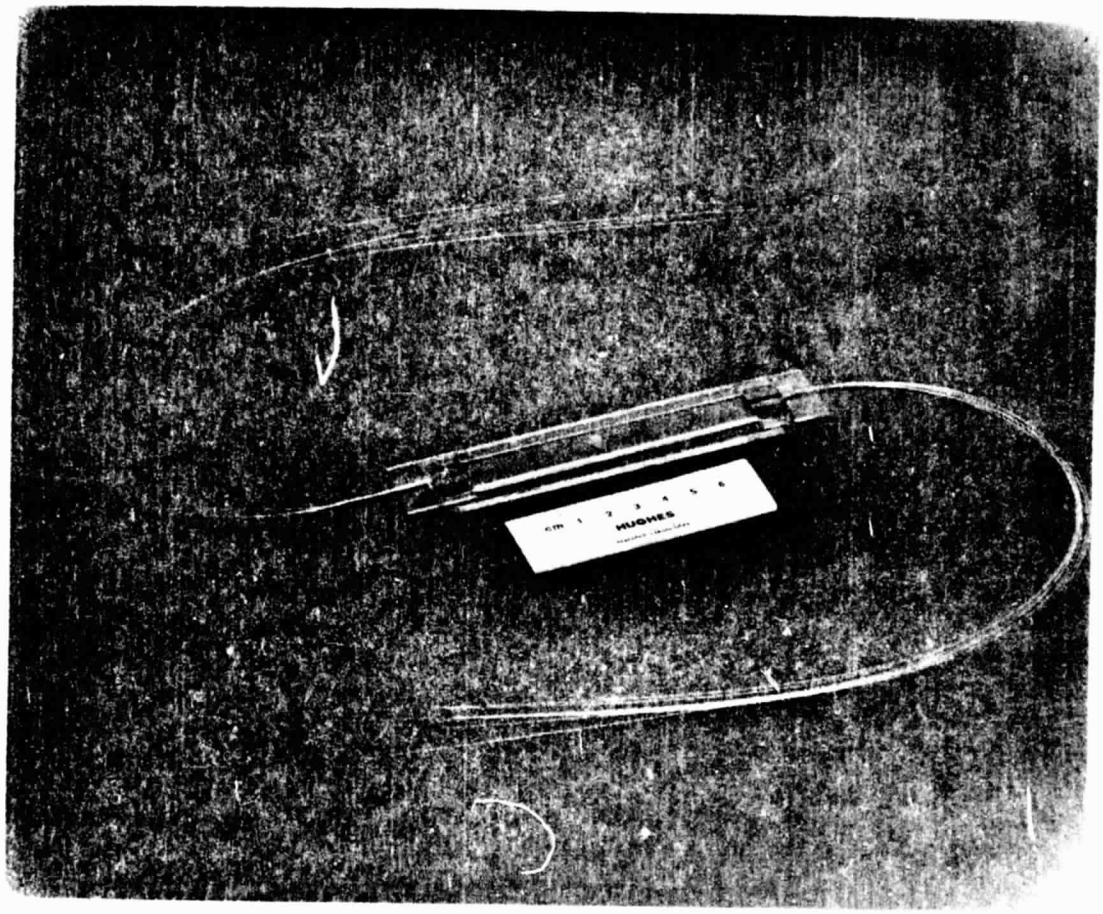

Fig. 5a. Planar transmission star coupler with eight-fiber ribbon epoxied to each end.

ORIGINAL PAGE IS
OF POOR QUALITY

ORIGINAL PAGE IS
OF POOR QUALITY

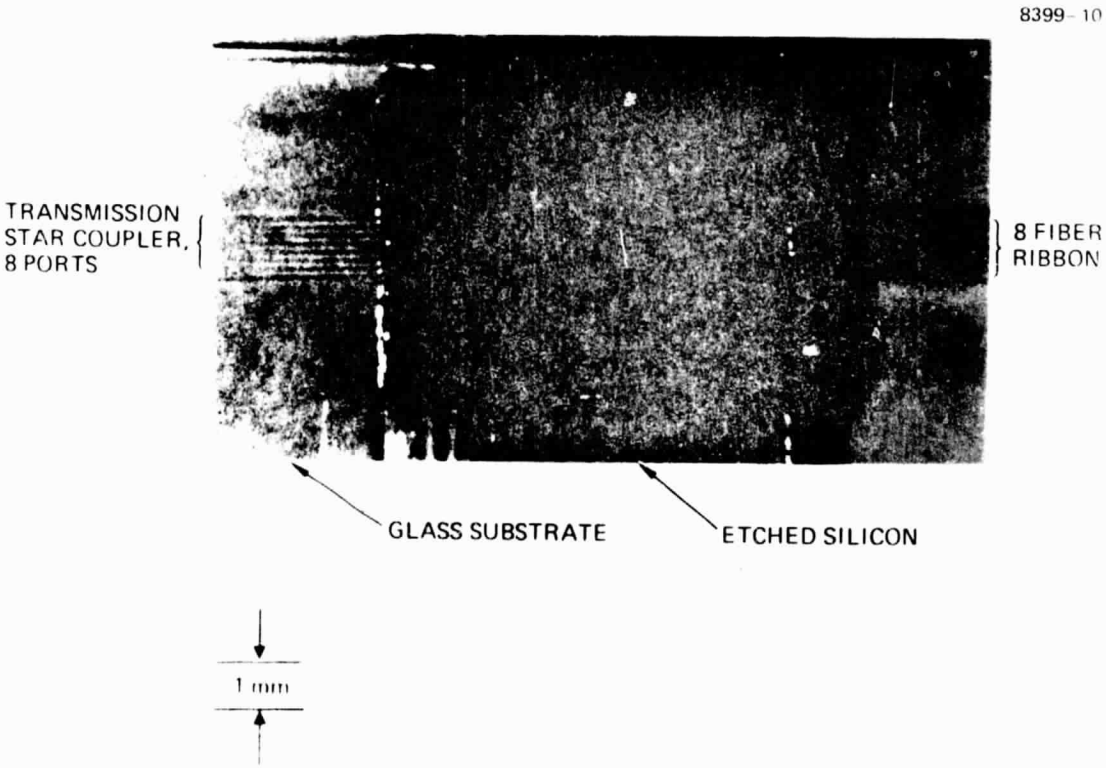

Fig. 5b. Closeup of transmission star fiber ribbon connection.

M12848 8453 7

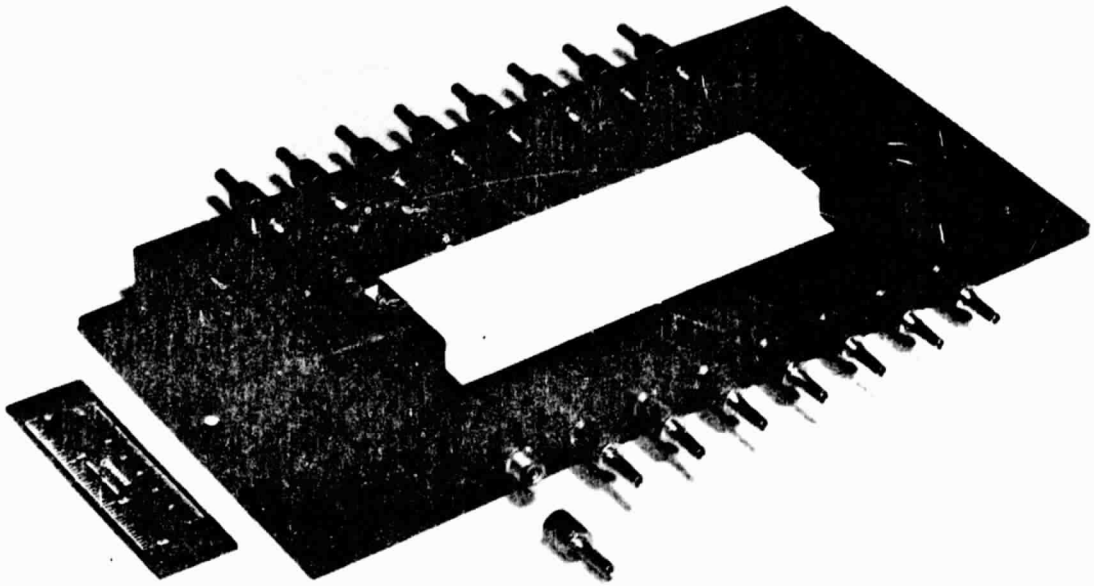

Fig. 6. Planar transmission star in box with fiber connectors (cover removed).

ORIGINAL PAGE IS
OF POOR QUALITY

M12847

ORIGINAL PAGE IS
OF POOR QUALITY

8453-8

Fig. 7. Planar transmission star in box with fiber connectors.

PRECEDING PAGE BLANK NOT FILMED

OPTICAL MEASUREMENTS

Optical measurements of the refractive index profile of the ion-exchanged channel, fiber-to-channel coupling effects, and the transmission star coupler throughputs are described here.

Refractive Index Profile

The refractive index profile of the ion-exchanged channel was examined. An interference microscope photograph of a thin section of three channels is shown in Figure 8. The highest index is 1.532, the region that directly contacted the melt, and the lowest is 1.523, that of the glass substrate. For a step index profile, these indices would correspond to an NA = .16.

Figure 8 clearly illustrates that ion exchange occurs under the Al-masked area, diffusing laterally as well as normally into the glass. The diffusion distance normal to the surface is $\sim$100 μm. Smaller mask openings would result in a more circular refractive index pattern.

We conclude that $\Delta n = 0.009$ is sufficiently large to be able to match the Δn of a common commercial fiber. The spatial or cross-sectional mismatch of indices between the fiber and the channel will, however, decrease the coupling efficiency to some extent. Processes for attaining closer cross-sectional index matching are under investigation at HRL.

Optimization of the Fiber-to-Channel Coupling

In order to determine the optimum width of a constant width channel for best fiber-to-channel-to-fiber and to determine the fiber-to-channel coupling losses, a series of measurements were made on existing slides of straight channels of varying widths. Channel widths (of the mask) of 25, 40, 50, 65, 80, 90, 250, 325, 500, and 620 μm and channel lengths of one inch were available on previously fabricated slides. The slides had been dipped into

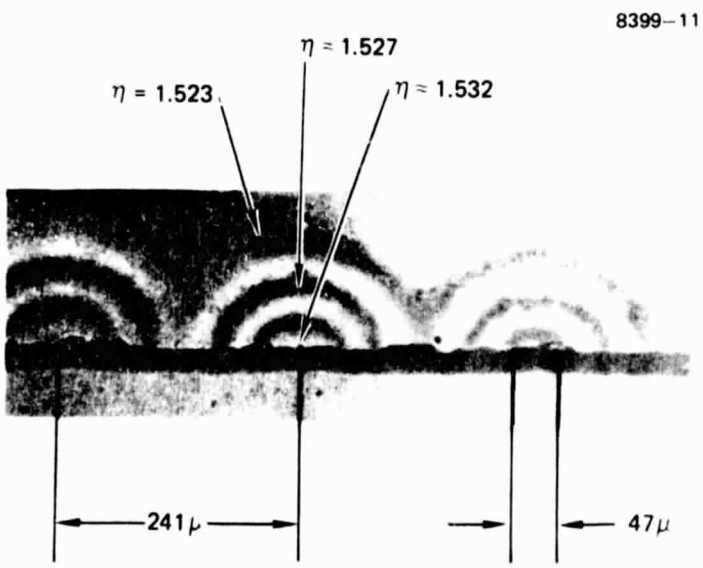

ORIGINAL PAGE IS
OF POOR QUALITY

Fig. 8. Interference microscope photograph of a star coupler cross section showing change of index of refraction. Center-to-center channel spacing and mask opening width are shown along with the indices of the substrate and ion exchanged channels.

the melt for twenty (20) minutes. The ion exchanged regions for various channel widths of the mask are shown schematically in the inset of Fig. 9. The diffusion of Li ions underneath the masks is indicated. The diffusion depth (∿100 μm) is determined by length of dipping (20 minutes) and melt temperature (580°C). Graded index fibers of 63 μm core and 125 μm o.d. were butt coupled to each end of a channel.

Our measurements indicated that maximum throughput for fiber to channel to fiber (∿35%) occurred over a broad range of widths, 45-80 μm, shown in Fig. 9 and indicated by F/C/F. The fiber-to-channel output versus channel widths are indicated by F/C in Fig. 9; the near field is focussed on a detector with a lens, with an iris to isolate the channel throughput from scattered light. The efficiency of coupling from the output channel to the fiber can then be estimated by taking the ratio of (F/C/F) to (F/C); the ratio is shown in Fig. 10 as a function of channel width, with a maximum of ∿75%.

In summary, we conclude that:

- Fiber-to-channel-to-fiber throughputs were measured to have a broad maxima of ∿35% for channel widths of 45 to 80 μm for the fabricated channels. This result includes channel scattering losses and channel-to-fiber coupling losses resulting from refractive index profile mismatch at both the input and output. The graded index fiber has core diameter of 63 μm, o.d. of 130 μm, and an NA of 0.14. Closer matching of profiles are desired, such as with buried channels.
- The output channel-to-fiber losses for channel widths of 45 to 80 μm are ∿25%.
- From the straight channel experiments, we can estimate that the power entering a star coupler is >57% with present processing. We expect that a well fabricated star coupler will have total throughput somewhat greater than the above value.

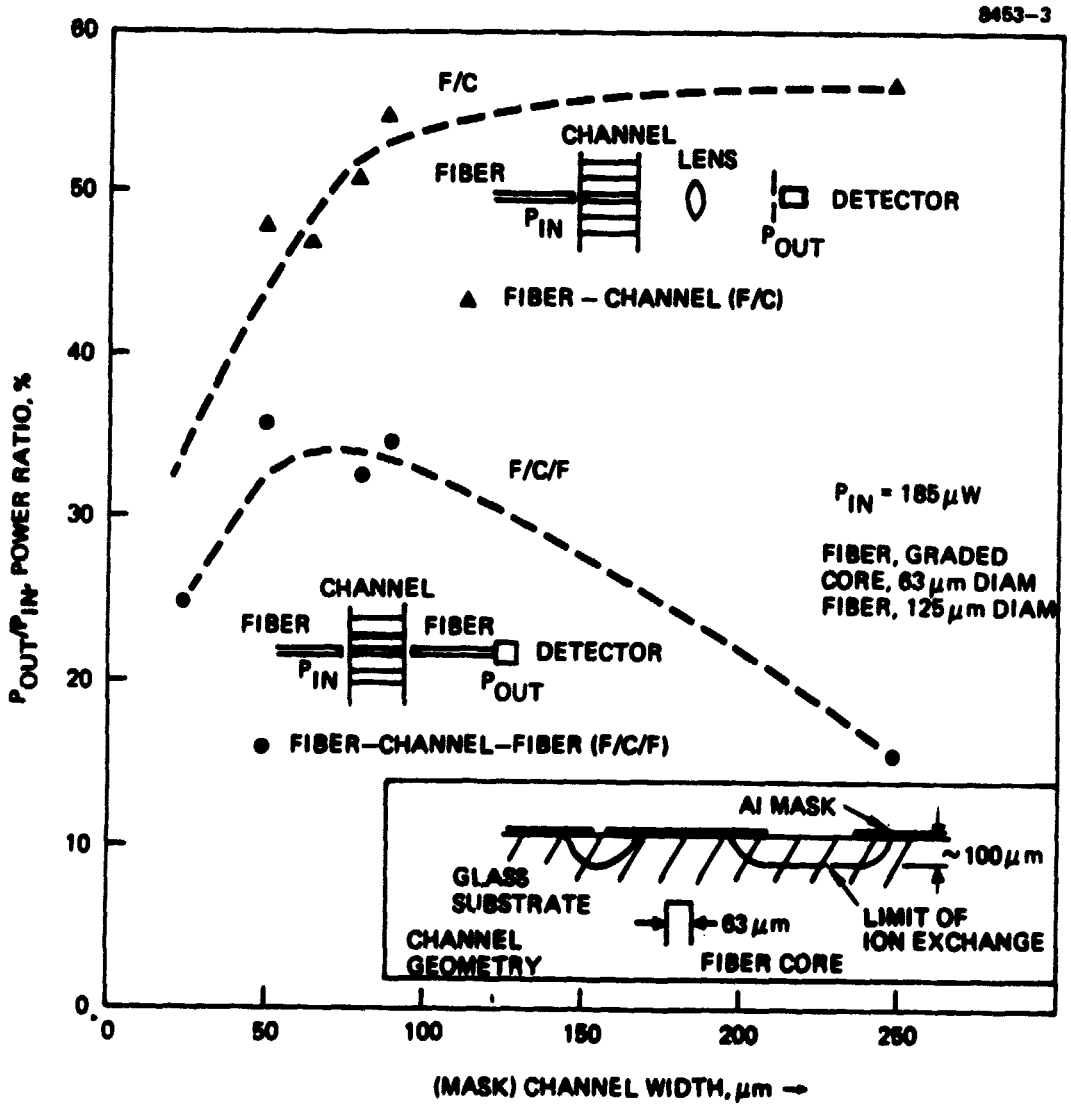

Fig. 9. Power transmission ratios of constant width channel vs. channel widths for fiber-to-channel coupling (F/C) and fiber-to-channel to-fiber coupling (F/C/F).

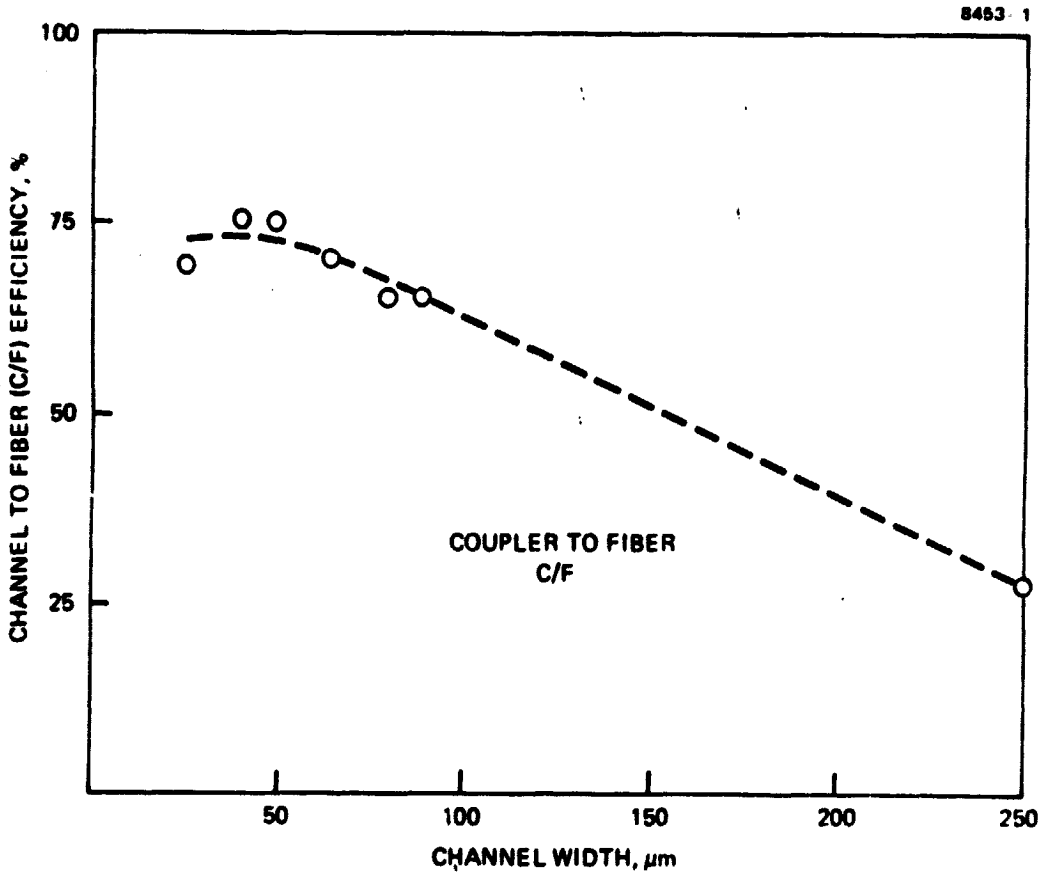

Fig. 10. Channel-to-fiber coupling efficiency versus channel widths.

Transmission Star Throughput

As mentioned above, the last set of ten transmission star couplers fabricated with the positive resist process has yielded the best quality stars thus far, with relatively low surface scattering. Plates containing the stars were immersed in the Li_2SO_4-K_2SO_4 melt for the following temperature and time intervals: 605°C, 5 min; 605°C, 10 min.; 605°C, 15 min.; 585°C, 20 min.; 585°C, 40 min. Two stars were located on each plate. The plate immersed for 20 min. at 585°C appeared to yield the best stars. Fairly clean near field output pattern is observed when light from a fiber is inputted into any of the entrance ports. With light from a fiber (∿200 μW) inputted into one of the entrance ports, the maximum sum total power intercepted by a fiber placed in sequence at the eight exit port was 24 μW (-9.2 dB). There are still considerable variations in the outputs of the eight exit ports, varying at best by a factor of three. The variations may be due to imperfection scattering, graded index structure boundaries, and/or lack of sufficient mixing lengths for the graded index structure. The cause of these variations is presently under investigation.

We attached an eight-fiber ribbon to each end of a transmission star (ion exchange process, 585°C for 20 minutes) with epoxy as described previously. During the attachment process, while the epoxy was still liquid, we have observed an increase in the throughput to as much as 28 μW (-8.5 dB). Part of this increase can be assigned to the elimination of the air gap; as the epoxy hardens, however, a slight decrease (∿5 to 10%) of throughput power is usually observed. Whether the decrease results from refractive index change of the hardened epoxy or from slight misalignment of the ribbon-to-channel connection as the epoxy hardens is not known at this time.

The 8 by 8 matrices shown in Table Ia represent the distribution of light from each input fiber to each of the output fibers for the ribbon-star-ribbon assembly prior to assembly in a breadboard box. The channels are numbered according to Figure 11. Table Ia shows the initial distribution matrix; Table Ib shows the distribution where the input and output are interchanged. The maximum total throughput of Table Ia is again 2.4 μW (-9.2 dB), where the power in the input fiber is ∿200 μW. The average total throughput is 18.1 μW (-10.4 dB). We note that one of the output channels is much lower than the average distribution, particularly with input into channels #1 and #8. We do not know the reason for this behavior at this time. It appears that a modification of the outer boundaries of the star, to compensate for the graded index of the mixing region, may correct the low output of the channel. The computer program for the graded index star is expected to clarify the result.

The lower matrix (with interchanged input and output) shows total outputs lower (∿-1 to -2 dB) than the upper matrix. At this research stage, we do not believe that this is significant. The stars were ion-exchanged in a vertical oven with possible thermal gradients in the melt. Inhomogeneous ion exchange could have resulted. Future stars are expected to show uniform reciprocal distributions as the process is improved.

The 8x8 distribution matrices of the planar star coupler assembled in a box with sixteen fiber couplers and sixteen pigtails as shown in Fig. 7 was measured and is given in Table IIa, and with input and output reversed in Table IIb. We recall that the matrix of Table Ia is that for the star with ribbon pigtails, that of Table IIa, b the same star plus ribbon, but with eight input and eight output fiber connectors. The average loss due to the two connectors is ∿-2.3 dB, or a loss of -1.2 dB per connector.

TABLE Ia. DISTRIBUTION MATRIX FOR 8x8 PLANAR TRANSMISSION STAR #1, WITH 2 SETS OF FIBER RIBBONS

OUTPUT #2 end / INPUT #1 end	1	2	3	4	5	6	7	8	Total Power μW
1	2.46	1.60	2.26	1.01	3.78	5.99	5.14	0.57	22.31
2	3.30	3.26	2.48	5.41	1.59	4.05	2.68	1.45	24.22
3	0.60	0.92	1.65	3.22	4.30	2.43	2.33	1.79	17.24
4	0.40	0.46	0.58	0.97	2.72	4.56	3.23	3.49	16.41
5	2.53	1.90	2.02	1.15	1.68	1.80	1.75	2.66	15.49
6	1.70	2.03	1.98	1.12	1.76	1.67	2.46	2.79	15.51
7	6.87	3.06	1.38	1.33	1.20	1.23	0.90	0.97	16.94
8	0.70	6.90	3.05	1.30	1.14	0.93	0.96	1.34	16.32
								Avg.	18.1 μW

TABLE Ib. SAME AS Ia, EXCEPT INPUT AND OUTPUT ARE REVERSED.

OUTPUT #1 end / INPUT #2 end	1	2	3	4	5	6	7	8	
1	3.59	2.38	0.85	0.54	1.48	1.24	1.77	0.68	12.55
2	3.29	3.18	0.86	0.69	1.00	1.68	0.85	1.45	13.0
3	3.20	3.61	1.42	0.37	0.52	0.78	0.56	0.67	11.13
4	2.50	4.60	3.25	0.64	0.30	0.51	0.63	0.69	13.12
5	10.70	2.50	1.81	1.38	0.55	0.82	0.40	0.46	18.62
6	3.49	5.00	1.43	1.42	0.72	0.88	0.41	0.36	13.71
7	2.37	2.33	1.49	0.56	1.28	1.75	0.47	0.33	10.58
8	0.35	2.30	0.98	2.78	2.51	1.39	0.72	0.50	11.53
								Avg.	13.03

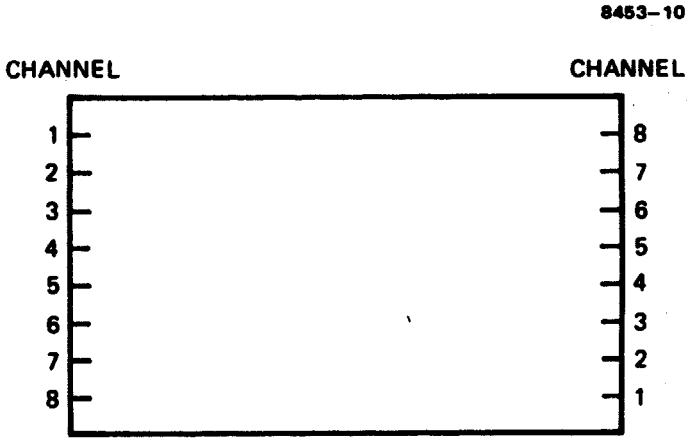

Fig. 11. Numbering of the channels of the transmission star coupler.

TABLE IIa. DISTRIBUTION MATRIX FOR STAR #1, BREADBOARDED IN A BOX, WITH FIBER CONNECTORS

output (white dot end) / input	1	2	3	4	5	6	7	8	Total µW Sum	Measurement
1	1.6	1.3	1.6	1.3	2.5	2.5	2.8	.50	14.1	14.40
2	1.6	1.5	1.5	3.7	1.1	2.9	1.6	1.0	14.9	15.60
3	.52	1.1	2.0	3.2	3.2	1.5	1.2	1.2	13.9	13.23
4	.33	.33	.46	.58	1.8	1.9	1.5	1.8	8.7	8.70
5	1.6	1.3	1.0	.91	1.3	1.4	1.3	1.8	10.6	10.93
6	1.0	1.1	.80	.56	.91	1.6	.96	1.6	8.5	9.87
7	2.0	1.7	.62	.91	.60	.41	.42	.45	7.1	7.65
8	.50	2.7	1.2	.60	.77	.42	.50	.80	7.5	8.20
							Avg.		10.7	11.1

TABLE IIb. SAME AS IIa EXCEPT INPUT AND OUTPUT REVERSED

output / input (white dot end)	1	2	3	4	5	6	7	8	Total µW Sum	Measurement
1	1.6	1.6	.57	.36	2.0	.67	2.0	.73	9.5	10.36
2	.85	1.4	.70	.26	.33	.60	.54	.67	5.4	6.50
3	2.1	1.9	1.3	.42	.59	.65	.22	1.0	8.2	8.93
4	.72	.9	1.7	.26	.47	.40	.32	.52	6.3	6.42
5	2.7	1.5	2.1	.81	.53	.57	.24	.40	8.9	9.45
6	1.2	2.6	.90	1.2	.86	.58	.22	.20	7.8	8.50
7	.93	6.1	6.3	.90	1.3	.68	.15	.22	6.6	8.20
8	.13	1.4	.93	2.3	1.74	.47	.38	.30	7.7	8.02
							Avg.		7.6	8.5

We wish to note that the matrix measurements of the boxed star were sensitive to movement of certain of the input pigtails and to launch conditions of the laser light. Whether this problem arises from distortion at the connector is not clear at this time, but the effect will be examined more fully and corrected.

We attached fiber ribbons to another 8x8 transmission star (in exchange process, 585°C for 20 minutes) and measured its distribution matrices as shown in Tables IIIa and b. The device is denoted as Star #2. Stars #1 and #2 were ion exchange processed at the same time on the same plate glass substrate. Comparing Tables I and III shows substantially the same results. One difference is the large relative output of channel 8 when channel 1 is excited in Table IIIa. Whether this arises from local waveguide defect is not clear at this juncture.

The highest throughput was down ∿-96 dB relative to the power in the input fiber. We can partition the loss as follows:

Measured Insertion Loss	=	Measured Coupling Loss	+	Estimated Propagation Loss	+	Estimated Internal Loss

or

$$9 \text{ dB} = 4.2 \text{ dB} + \left(0.1 \frac{\text{dB}}{\text{cm}}\right)\left(8 \text{ cm}\right) + [4.0 \text{ dB}] \quad .$$

The measured coupling loss of 4.2 dB was determined from the experiments with parallel channels described above. The remainder of the insertion loss is partitioned to propagation loss and the internal loss of the star structure. If the propagation loss is taken to be very small (0.1 dB/cm), an estimated internal loss of 4.0 dB remains. The latter loss may be compared with the packing fraction loss of 3.8 dB for a linear array of fiber. We expect that the fiber to star coupling loss can be reduced to ∿0 dB with proper matching of index profiles, thereby resulting in an insertion loss of ∿5 dB.

TABLE IIIa. DISTRIBUTION MATRIX FOR 8x8 PLANAR TRANSMISSION STAR #2 WITH 2 SETS OF FIBER RIBBONS

input (X) \ output	1	2	3	4	5	6	7	8	Total μW Sum	Total μW Measurement
1	1.1	.83	2.5	2.1	2.3	3.2	1.0	6.4	19.4	21.0
2	2.1	1.7	3.8	5.4	1.7	3.1	1.2	1.7	20.7	22.3
3	.80	.95	2.5	3.4	5.2	2.4	3.8	1.2	20.3	22.3
4	1.4	1.4	1.8	2.4	2.0	4.7	2.5	3.4	19.6	17.8
5	.87	1.4	1.3	1.2	1.1	2.4	1.4	3.3	13.0	12.3
6	6.1	2.6	1.6	1.6	2.0	1.3	1.4	.98	17.6	16.3
7	7.4	5.6	2.1	.76	1.2	.70	.63	.76	19.2	18.8
8	.68	8.0	3.3	3.6	1.7	.96	1.4	1.7	21.3	21.2
								Avg.	18.9	19.0

TABLE IIIb. SAME AS IIIa EXCEPT INPUT AND OUTPUT ARE REVERSED

input \ output (X)	1	2	3	4	5	6	7	8	Total μW Sum	Total μW Measurement
1	.87	1.1	.42	.75	.61	3.8	13.4	.78	21.7	22.4
2	.48	.82	.46	1.3	.77	1.5	5.6	7.0	17.9	17.6
3	1.7	1.9	2.3	1.8	.93	1.4	2.7	2.3	15.0	14.6
4	1.7	1.1	1.6	2.4	1.2	1.4	.84	2.7	12.9	13.5
5	2.1	1.7	3.3	3.5	.95	1.5	.82	1.8	15.7	15.7
6	2.1	6.8	2.2	4.0	.96	.74	.62	.99	18.4	18.6
7	3.8	3.0	3.3	1.5	.78	.99	.42	.77	14.6	15.5
8	4.6	2.3	1.4	2.8	1.9	.75	.61	1.1	15.5	14.6
							Avg.		16.4	16.6

CONCLUSIONS

- Manufacture of planar distribution couplers for optical fibers where the planar structure is fabricated by an ion diffusion process has been demonstrated.
- Mechanically solid coupler-fiber ribbon-connector assembly possible for future spacecraft applications have been demonstrated.
- No restriction on the number of fiber terminals appears to be valid. Multiple couplers may be used in series.
- Further improvement of the couplers to -5 dB transmission loss [plus connector loss ($\sim$1.2 dB/connector)] appears to be attainable.
- Precise equal partitioning of light appears to be possible.

APPENDIX A

DESIGN OF PLANAR STAR COUPLERS FOR FIBER OPTIC SYSTEMS

O. G. Ramer

PRECEDING PAGE BLANK NOT FILMED

ABSTRACT

A horn structure within a planar fiber optic star coupler has been shown by computer design to significantly reduce if not eliminate the packing fraction loss associated with the coupler geometry. The ray tracing design procedure is used to characterize the partitioning of light to the various ports and the losses are tabulated. An eight port planar star is used to illustrate the design capabilities.

INTRODUCTION

Low loss multimode fiber optic components are a key to successful multimode fiber optic systems. The technique of fusing individual fibers together[1,2,3] to make low loss T couplers has resulted in reproducible couplers but the yield of packaged devices is low, suggesting high unit costs. Fiber optic star couplers[4,5] are successfully made by a number of techniques, however the packing fraction loss remains a problem. A planar approach of making these couplers is being pursued. It is believed that high yield and low cost can be achieved. This paper describes a

ray-tracing investigation of the multimode planar star coupler illustrated in Fig. 1. This investigation was made in order to characterize the partitioning of light into the planar branches as a function of index profile, device dimensions and configuration; the losses are also tabulated. Computer ray tracing has been used to identify the important design parameters for the planar star. Example parameters are the required mixing length for equal partitioning of light into each of the channels and the horn angle required to significantly reduce the packing fraction losses. It should be pointed out that straight line ray tracing requires that the planar guides and the substrate be uniform in refractive indices. The ray tracing analysis is limited to such planar structures.

RAY TRACING PROCEDURE

In order to accurately simulate the devices, the rays must statistically simulate the total of the modes in the guides. Since the structure that is analyzed is a step index configuration, we have elected to choose the rays randomly such that the angular extent of the numerical aperture is filled uniformly. Although it is also possible to randomly choose the initial x and y position of the rays in some z plane, we elected to divide the input plane into a rectangular mesh and trace a single ray from the center of each rectangle. Using this algorithm and starting the random number generator at different positions does not affect the final result significantly (<1% variation) if a large number (>5000) of rays are traced. That is, some average properties associated with the motion of a large number of identical systems differing over a range of initial conditions is obtained.

Given the initial values for position (x,y) and direction cosines (k, l, m) of a ray at some $z_0(=0)$ it is possible, in general, to solve for its position and direction cosines at any other value of z. Although ray tracing is well understood the procedure is described.

Snell's law describes the refraction of light through an interface (Fig. 1) and is given by

$$n_2 \bar{S}_2 \times \bar{G} = n_1 \bar{S}_1 \times G \tag{1}$$

or

$$(n_2\bar{S}_2 - n_1\bar{S}_1) \times \bar{G} = 0 \tag{2}$$

where

S_1 is a unit vector in the direction of the ray impinging on the interface

$\bar{G}$ is a unit vector in the direction of the local normal to the interface

n_1 and n_2 are the refractive indices on the two sides of the interface

$\bar{S}_2$ is a unit vector in the direction of the ray after refraction and/or reflection ($n_1 = n_2$) at the interface.

Equation (2) is a simple vector relation which can be solved exactly; it is satisfied if the vector in the parentheses is colinear with $\bar{G}$, thus allowing one to write

$$n_2\bar{S}_2 - n_1\bar{S}_1 = \Gamma\bar{G} \tag{3}$$

or

$$n_2\bar{S}_2 = n_1\bar{S}_1 - \Gamma\bar{G} \tag{4}$$

where Γ is yet an unknown quantity. The dot product of Eq. (4) with itself eliminates the unknown $\bar{S}_2$ and gives the following quadratic equations in Γ:

$$\Gamma^2 - 2\Gamma(n_1\bar{S}_1 \cdot \bar{G}) + (n_1^2 - n_2^2) = 0 \tag{5}$$

or

$$\Gamma = n_1\bar{S}_1 \cdot G_1 \pm \sqrt{(n_1\bar{S}_1 \quad \bar{G})^2 - n_1^2 + n_2^2}\ . \tag{6}$$

By the appropriate choice of Γ, all situations that are encountered at a refractive interface can be accurately described. If the square root is imaginary ($n_1 \neq n_2$), the ray is totally internally reflected and the positive sign is chosen after setting $n_1 = n_2$

$$\bar{S}_2 = \bar{S}_1 - (2\bar{S}_1 \cdot \bar{G})\bar{G}. \tag{7}$$

If the square root is real, the smaller absolute value of Γ will give the $\bar{S}_2$ corresponding to the physical situation of refraction (Fig. 3). Substitution of this value for Γ into Eq. (4) gives the new ray direction $\bar{S}_2$. In the analysis rays of this sort are lost from the device and thus summed to evaluate the losses.

The algorithm for ray tracing through a device is

a) initialize ray,

b) determine surface of intersection,

c) apply Eq. (7) if square root in Eq. (6) is imaginary. If square root is real, sum the ray as lost and go to (a)

d) repeat (b) and (c) until ray exits device,

e) sum ray as exiting appropriate port and to to (a).

The parameters of interest for star design are (see Fig. 1):

θ = half angle of taper angle,

X_T = half width of wall,

X_B = half width of channel,

Y_B = half thickness of film,

z = mixing length,

Numerical aperture of the guide,

Index of the surrounding region,

Number of ports N.

In the above algorithm the ray intersections with the guide boundaries remains to be defined. There are five independent sections (input guides, output guides, input horns, output horns, and mixing region) of the planar star. Each has to be handled separately with the appropriate coordinate transformation between regions. The coordinate system for each individual guide (horn, mixing region, etc.) is a z axis that bisects the guide with transverse x, and y axis. The x axis is parallel to the plane of the substrate.

Let the ray position be given by

$$\overline{P} = x\,\overline{I} + y\,\overline{J} + z\,\overline{k} \tag{8}$$

and the ray direction by

$$\overline{S} = \ell\,\overline{I} + m\,\overline{J} + n\,\overline{k} \tag{9}$$

If we are in any of the three uniform regions (input guide, output guide or the mixing region) the next boundary intersection, $\overline{P}_I$, is given by

$$\overline{P}_I = \overline{P} + \overline{T}\,D \tag{10}$$

where D is the smallest of the following three distances:

a) the distance to the x plane

$$DX = (x - \ell X_G/|\ell|)/\ell \tag{11}$$

b) the distance to the y plane

$$DY = (y - m\,Y_G/|m|)/m \tag{12}$$

and c) the distance to the end of the guide

$$DZ = (z - z_{max})/n \tag{13}$$

where $2x_G$, $2y_G$ and z_{max} are the guide dimensions. For example, in the mixing region

$$X_G = (X_B + X_T)N \tag{14}$$

$$Y_G = Y_B \tag{15}$$

$$z_{max} = z_{mix} \tag{16}$$

In the horns the next boundary intersection (Eq. 10) is given by the shortest distance between the y plane (Eq. 12), the end of the horn (Eq. 13) $z_{max} = X_T/\tan\theta$ or one of the two horn boundaries.

$$D = \frac{X - (Mz + B)}{Mn - \ell} \tag{17}$$

where for the input horns

$$M = \pm \tan\theta \tag{18}$$

$$B = \pm X_B \tag{19}$$

and for the output horns

$$M = \pm \tan(-\theta) \tag{20}$$

$$B = \pm (X_B + X_T) \tag{21}$$

This completes the ray tracing algorithm.

RAY TRACE ANALYSIS

n the ray trace program, rays can be input at any of the N ports; the program outputs are the number of rays that exit each of the ports and the number of rays that are lost. Figure 3 shows the result of varying the mixing length, Z, for an eight-port star coupler; each line represents the number of rays that exit a given port. The number of rays to each of the ports with ports 1 through 4 for input and $Z/X_B = 2750$ are given in Table 1. The number of rays lost or not satisfying the condition for total internal reflection at any one of the guide wall intersections is also given in Table 1. A total of 10,000 rays were traced for each input.

The major loss in conventional star couplers is the packing fraction loss. The purpose of the horn structure in the planar star coupler is to provide a means to reduce this loss. The losses for an eight port star have been calculated with the horn angle, θ, as a variable. The result of this calculation is shown in Fig. 4. For a horn angle equal to or

TABLE 1.

Input port / Output port	1	2	3	4
1	1195	999	927	905
2	967	942	922	957
3	948	934	964	1065
4	952	1014	1072	1053
5	891	967	1084	1077
6	966	991	992	1082
7	1020	988	1002	918
8	1162	1107	997	884
Loss	1999	2058	2040	2059
Total	10,000	10,000	10,000	10,000

greater than half the numerical aperture (NA/2) of the guide the loss is equal to the structure packing fraction. In this case the loss is

$$X_T/(X_T + X_B) = .75 \tag{21}$$

At reduced angles the loss is substantially reduced. The packing fraction loss for horn angles larger than NA/2 can be easily understood. Any ray that strikes the horn boundaries will have its direction changed by an angle equal to twice the horn angle. Hence for any horn angle larger than NA/2 the ray angle after striking the horn will be larger than the guide NA and lost. Reduced horn angles result in an adiabatic transition and reduced loss.

In conclusion the planar star coupler design presented shows that the packing fraction loss of the planar star copuler can be decreased. This is achieved by tapering the input guides with a taper angle less than half the numerical aperture of the guide. The mixing region length can be chosen for equal coupling to all ports. An experimental investigation is presently underway and the results will be reported in a separate article.

The author appreciates the critical reading of the manuscript and suggestions of Dr. C. K. Asawa. The stimulating discussions of Dr. M. K. Barnoski and Dr. G. L. Tangonan are also acknowledged.

FIGURE CAPTIONS

1. Schematic of a transmissive planar star coupler. Rays from the left are partitioned in the mixing region and exit from the guides at the right. The F_i indicate the fractional transmission to the ith output port.

2. Illustration showing that the appropriate choice of Γ in the solution of Snell's law is ρ_{min}.

3. Fractional transmission of an eight-port planar star coupler versus the mixing length. The fractional transmission to port i is labeled F_i.

4. Fractional loss of an eight port star versus the horn angle, θ. The loss of 75% is the structure packing fraction.

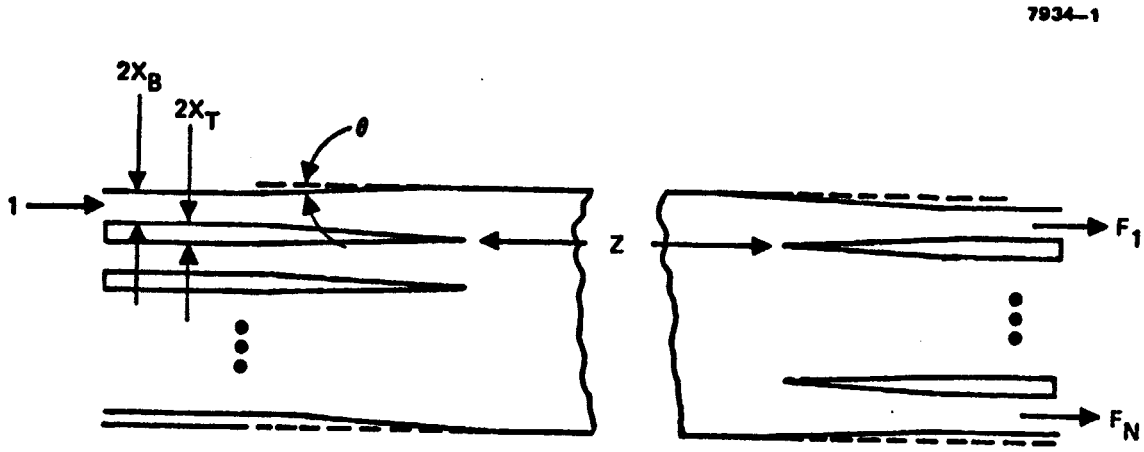

THICK FILM, THICKNESS $2y_B$

7508-3

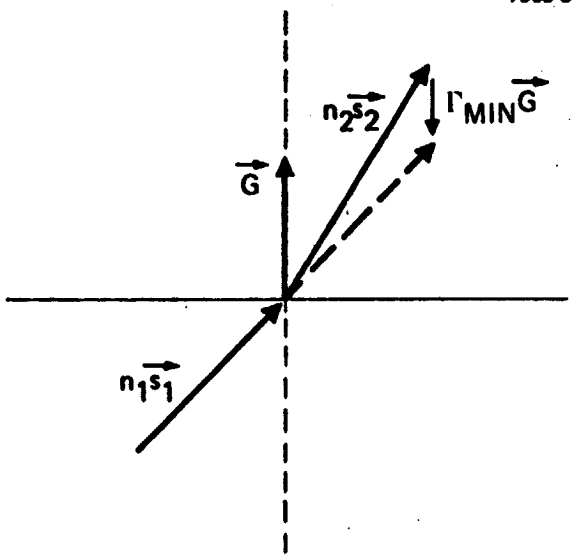
$n_2\vec{s}_2$
$\Gamma_{MIN}\vec{G}$
$\vec{G}$
$n_1\vec{s}_1$

(a)

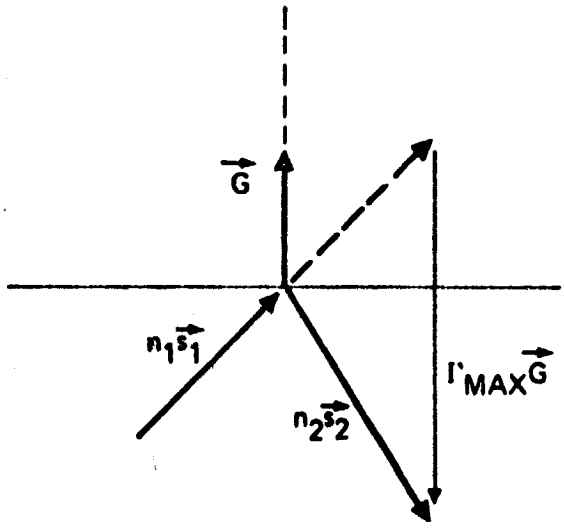
$\vec{G}$
$n_1\vec{s}_1$
$\Gamma_{MAX}\vec{G}$
$n_2\vec{s}_2$

(b)

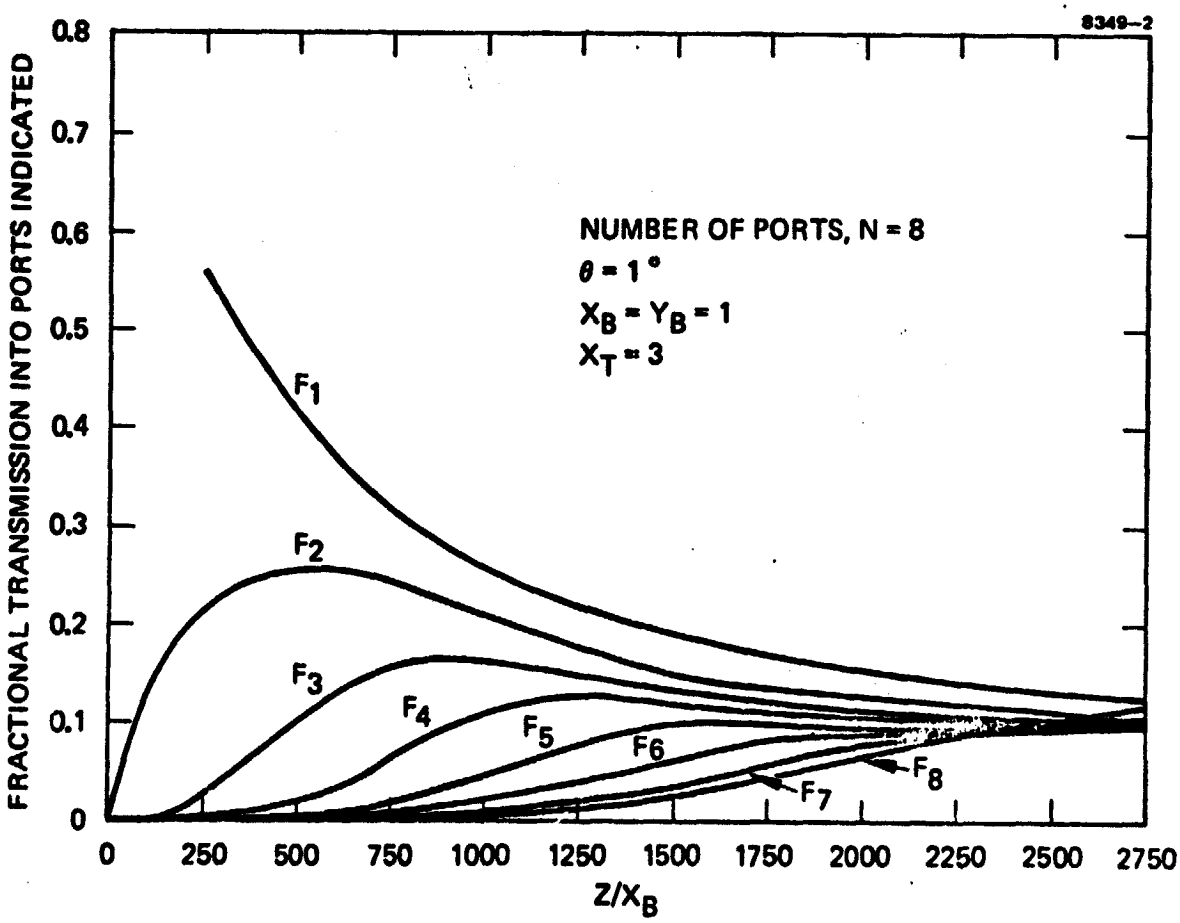
8349-2
FRACTIONAL TRANSMISSION INTO PORTS INDICATED
0.8
0.7
0.6
0.5
0.4
0.3
0.2
0.1
0
NUMBER OF PORTS, N = 8
θ = 1°
X_B = Y_B = 1
X_T = 3
F1
F2
F3
F4
F5
F6
F7
F8
0
250
500
750
1000
1250
1500
1750
2000
2250
2500
2750
Z/X_B

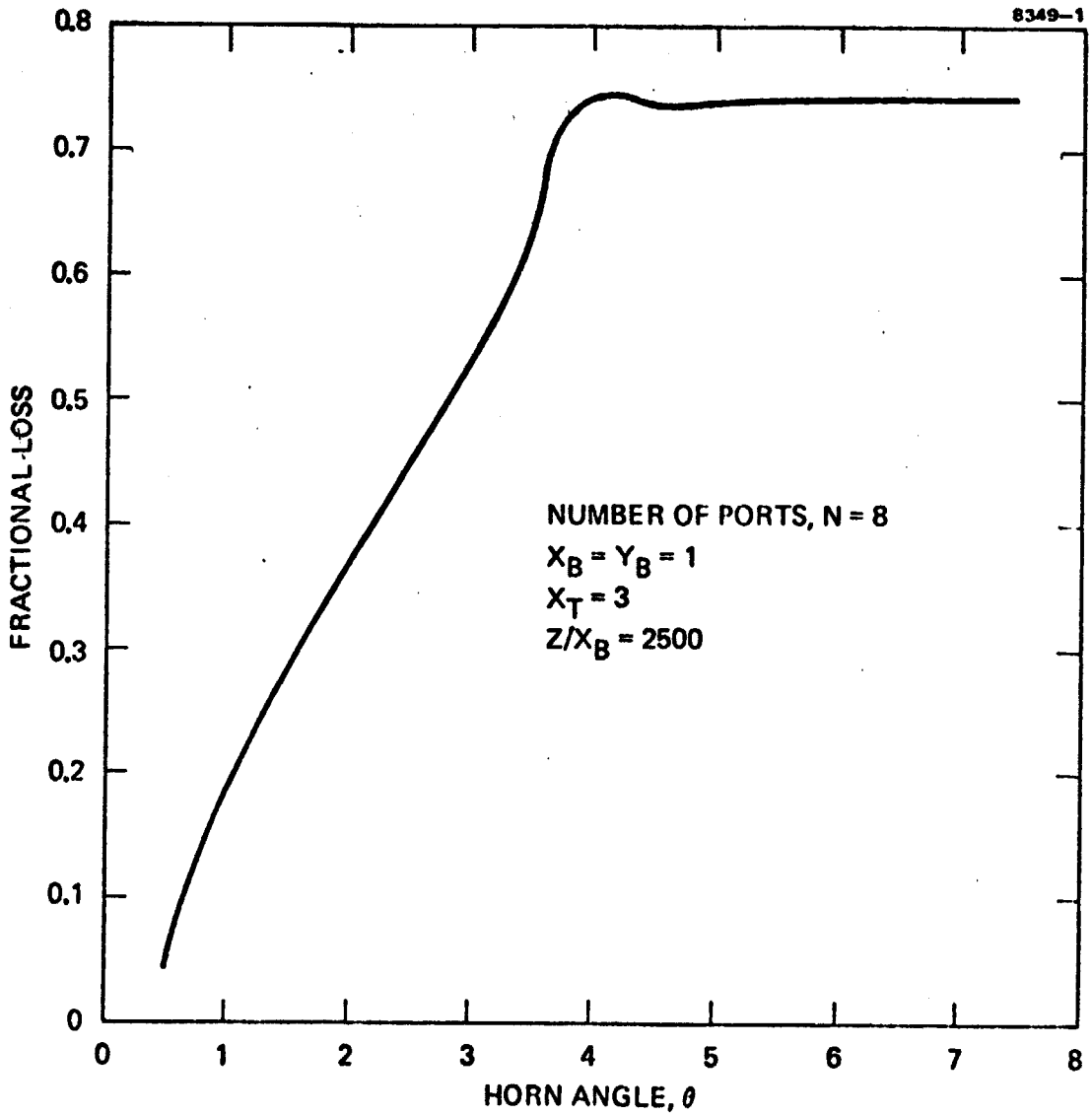
8349-1
0.8
0.7
0.6
0.5
0.4
0.3
0.2
0.1
0
FRACTIONAL LOSS
NUMBER OF PORTS, N = 8
$X_B = Y_B = 1$
$X_T = 3$
$Z/X_B = 2500$
0
1
2
3
4
5
6
7
8
HORN ANGLE, θ

PRECEDING PAGE BLANK NOT FILMED
PRECEDING PAGE BLANK NOT FILM...

APPENDIX B

ORIGINAL PAGE IS OF POOR QUALITY

PLANAR MULTIMODE COUPLERS FOR FIBER OPTICS

G.L. TANGONAN, L.E. GORRE and D.L. PERSECHINI
Hughes Research Laboratories, 3011 Malibu Canyon Road, Malibu, CA 90265, USA

Received 10 August 1978

Ion exchange in a melt of lithium and potassium sulfates is utilized to form couplers for multimode fiber optics. The results of coupling measurements on asymmetric Y-branch couplers are given.

For multimode fiber optic systems couplers or taps are necessary for data distribution to several terminal users. Couplers are presently made with the help of optical fibers (fusing, tapering, lapping and gluing) or with microoptic components such as microlenses and beam splitters. Good couplers have been demonstrated with all these methods.

Multimode couplers can also be made by planar processing. In principle, the planar approach utilizing photolithographic processing is promising because of its versatility and high reproducibility. Auracher et al. [1] have reported the first planar branching networks formed in photo-polymer materials of 100 μm thickness. We have formed planar coupling structures for multimode guides using the ion exchange process described by Chartier et al. [2]. In this process an eutectic mixture of Li_2SO_4 and K_2SO_4 is heated under an oxygen atmosphere to 580°C. A sodium glass slide is suspended over the melt for 30 minutes to reach thermal equilibriation with the melt. It is next dipped into the melt for 20 minutes, then again suspended over the melt for 10 minutes to avoid any thermal shock. Planar waveguides, 100 μm deep, are made by this process. The coupler structures are formed by masking with a thick Al film (1 to 2 μm). The Al mask is subsequently removed by dipping the slide in hot 6 M HCl solution. Degradation due to aging was not observed, unlike the Ag ion exchange processes in glass [3].

An investigation of reactions between the melt and the glass during the process was carried out. Our study on the melt showed that SO_3 was continually produced. Li_2SO_4, which is less thermally stable than K_2SO_4, was decomposing to Li_2O, which is corrosive to SiO_2. The addition of Li_2O to SiO_2 to form Li_2SiO_3 explains the observed thinning of the slide by 2 μm after 20 minutes of exchange. It would be difficult to attribute this thinning solely to a simple exchange process.

Whether the increase in refractive index is due exclusively to an ion exchange of Li^+ for Na^+ has not

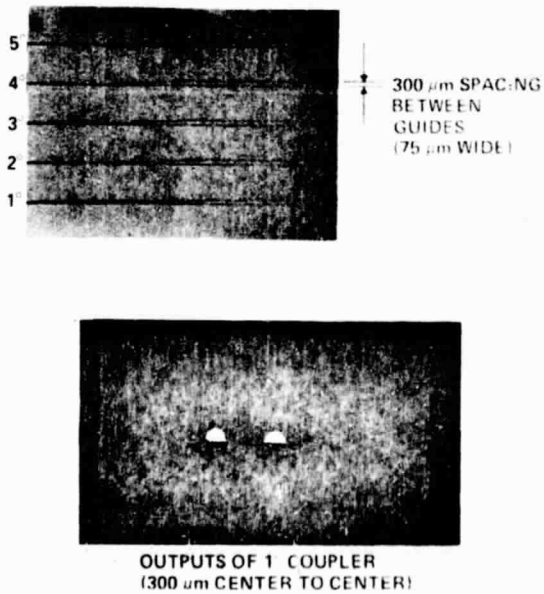

Fig. 1. Planar coupler array formed by ion exchange in a glass slide.

been ascertained. Other exchange processes such as K^+ for Na^+[4] or addition of Li_2O [5] may be occurring. The relative contributions of these other mechanisms have not been determined. Experiments using selected lithium and potassium salts (LiCl and KCl, for instance) are being conducted to determine the importance of these effects.

In fig. 1 we show a top view of an ion exchange slide with coupling structures formed using 1, 2, 3, 4 and 5° branches. The coupling branches are continued parallel to the main branch when 300 μm separation is attained. This facilitates the power measurement because the optical fibers placed at the output ports may be perpendicular to the slide end face. The output of the 1° branch is shown also in fig. 1. Using graded index fibers (Corning) of 65 μm core size the coupling ratios were measured from fiber input to fiber output with the planar coupler in between. Mode strippers were used to ensure that only guided modes were measured. The results are shown in fig. 2, where for two outputs P_1 and P_0 we have graphed $P_1/(P_1 + P_0)$ where P_1 is the branch output and P_0 is the straight output. A clear trend of decreasing coupling with increased branching angle is observed. The error bars are due mainly to the experimental difficulties in fiber placement precision and processing variations. To demonstrate further the versatility of the planar coupler approach a tapered coupler structure has been formed as shown in fig. 3. The coupling is controlled by varying the parameters d_2, θ_1, θ_2 and θ_3. For d_1

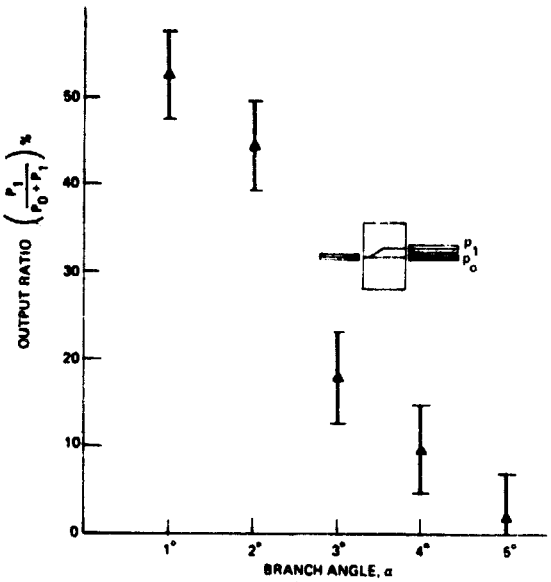

Fig. 2. Coupling ratio results for different branch angles.

= 75, d_2 = 50, d_3 = 100 μm and θ_1 = 2°, θ_2 = 0.66°, and θ_3 = 1°, a coupler with 20:1 tap ratio was measured.

The ion exchange process seems well suited for fiber optic coupler applications, in fact, the guide losses we have observed are quite low. We estimate that the guide losses are 0.1 to 0.5 dB/cm depending on

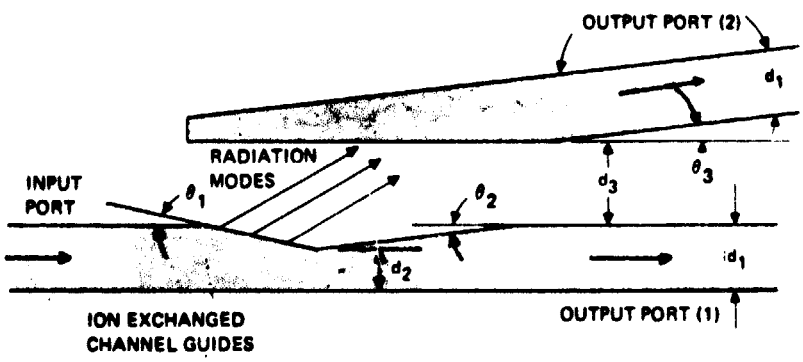

Fig. 3. Tapered couplers of planar variety formed by ion exchange. Coupling is due predominantly to radiation mode excitation by the taper.

processing variations. The dominant scattering mechanism is due to surface cracks, which have been largely eliminated by preprocessing of the slide. The crack density is diminished by a process involving a 5 min etching of the slide in 5% aqueous HF. In addition, a fire polishing of the slides prior to ion exchange reduces the final crack density. A detailed description of these results will be published later [6].

Several problem areas must be addressed which deal with optimization of the coupling efficiency from fiber to planar coupler, device packaging (affixing the pigtails), and guide formation reproducibility. Our best results on excitation of the channel guides with graded index fibers give only a 65% coupling efficiency. The processing used was 30 min diffusion at 580°C with a 65 μm channel width opening. At present this is the dominant loss figure. It is clear from fig. 1 that the output intensity profile must be modified to better approximate that of a fiber to improve the coupling. Careful control of the diffusion conditions will certainly enhance this figure, especially when buried structures are obtained by a second exchange process wherein K is re-introduced into the glass, subsequent to the Li exchange.

In conclusion we have demonstrated the feasibility of the ion exchange process in forming deep multimode guide structures for fiber optic coupler applications.

The authors wish to thank Drs. M.K. Barnoski, O.G. Ramer, C.K. Asawa, G.R. Blair and R.C. Pastor for their encouragement and advice.

References

[1] F. Auracher, H. Boroffa and R.Th. Kersen, Tech. Digest of the Integrated Optics Conference, January 1976, Utah, paper MD6-1.
[2] G.H. Chartier, P. Jassaud, A.D. de Oliviera and O. Parriaux, Elect. Lett. 13 (1977) 763.
[3] T.G. Giallorenzi, E.J. West, R. Kirk, R. Gunther and R.A. Andrews, Appl. Optics 12 (1973) 1240.
[4] W.G. French and A.D. Pearson, Ceramic Bulletin 49 (1970) 974.
[5] H.M. Garfinkel, J. Phys. Chem. 72 (1968) 4175.
[6] G.L. Tangonan, L.E. Gorre and D.L. Persechini, to be published.